Tapers for Large Planar Phased Arrays on Regular Grids: Simple Design Methods versus Second-Order Cone Programming

Jeffrey O. Coleman

Naval Research Laboratory, Radar Division
Washington D.C., USA
http://alum.mit.edu/www/jeffc

ABSTRACT

Design experiments compare taper-design approaches for a narrowband planar array of 10,000 or so elements on the triangular grid. Considered: a hexagonal-kernel McClellan transformation, a product of three 1D tapers, sampling Taylor's circular aperture, and second-order cone programming.

1. INTRODUCTION

Simple ways exist for designing element weights—a taper—for a large narrowband planar phased array, *e.g.* two or more 1D tapers are multiplied or a continuous distribution such as Taylor's circular aperture [1] is sampled. Is this adequate? Can modern SOCP optimization improve performance?

Here simple example taper designs are compared to optimal designs for an array of nearly 10,000 elements on a triangular grid. Overlapping subarrays make such large tapers unnecessary today, but this may change as per-element costs decline further, and here large size favors simple methods.

Notation and plotting conventions are established next. Then Section 3.1 and Section 3.2 compare design approaches for arrays with hexagonal and circular outlines respectively. Major results plots are collected at the end, as Figs. 3 and 4, even though discussion of them begins before Figs. 1 and 2.

2. THEORY, NOTATION, AND GEOMETRY

2.1 A signal-processing view of basic array theory

A moveable antenna at position $\mathbf{x}$ has output $a(\mathsf{t},\mathbf{x})$, an LTI and space-invariant function of incident fields, the latter since replacing $\mathsf{fields}(\mathsf{t},\mathbf{x})$ with $\mathsf{fields}(\mathsf{t},\mathbf{x}-\mathbf{x}')$ replaces $a(\mathsf{t},\mathbf{x})$ with $a(\mathsf{t},\mathbf{x}-\mathbf{x}')$ assuming no nearby field-disturbing objects. Sample spatially at nominal element position $\mathbf{x}=\lambda\mathbf{B}\boldsymbol{n}$ to obtain $a(\mathsf{t},\lambda\mathbf{B}\boldsymbol{n})$, where the columns of dimensionless 3×2 basis matrix $\mathbf{B}$ are basis vectors, λ is upper-band-edge wavelength, and where integer two-vector $\boldsymbol{n}$ indexes elements. Practicality requires the antenna structure to be periodic to be unchanged by this repositioning. Unused, terminated "guard elements" at array edges make elements used "feel" electromagnetically like they are in an infinite, truly periodic array.

Incident fields from far-off sources are integral combinations of plane waves $e^{j(\omega\mathsf{t}-\mathbf{k}\cdot\mathbf{x})}$ parameterized by ω and wavenumber vector $\mathbf{k}$. These are LTSI-system eigenfunctions, so the pre-sampling output is that integral with waves scaled by a complex eigenvalue depending on ω and $\mathbf{k}$.

Spatial sampling will replace $\mathbf{x}$ with $\lambda\mathbf{B}\boldsymbol{n}$ across the integral, so we'll want spatially sampled plane waves in a convenient form. Write $e^{j(\omega\mathsf{t}-\mathbf{k}\cdot\mathbf{x})}$ as $e^{j2\pi(\mathsf{ft}+\boldsymbol{\ell}^\mathsf{T}\mathbf{x}/\lambda)}$ using dimensionless vector $\boldsymbol{\ell}$, in the direction of arrival (DOA) when $\mathsf{f}>$

0, and sample at $\mathbf{x}=\lambda\mathbf{B}\boldsymbol{n}$ to obtain $e^{j2\pi(\mathsf{ft}+\boldsymbol{\ell}^\mathsf{T}\mathbf{B}\boldsymbol{n})}$. Then write $\boldsymbol{\ell}=\underline{\boldsymbol{\ell}}+\boldsymbol{\ell}_\perp$ using array-plane and normal components to make this $e^{j2\pi\mathsf{ft}}e^{j2\pi\underline{\boldsymbol{\ell}}^\mathsf{T}\mathbf{B}\boldsymbol{n}}$ using that $e^{j2\pi\boldsymbol{\ell}_\perp^\mathsf{T}\mathbf{B}\boldsymbol{n}}=1$ from the orthogonality of $\boldsymbol{\ell}_\perp$ to the basis-vector columns of $\mathbf{B}$. Finally, change variables using two-vector $\boldsymbol{f}=\mathbf{B}^\mathsf{T}\underline{\boldsymbol{\ell}}$, inverted by $\underline{\boldsymbol{\ell}}=\mathbf{B}^{+\mathsf{T}}\boldsymbol{f}$, where Moore-Penrose pseudoinverse $\mathbf{B}^+\triangleq(\mathbf{B}^\mathsf{T}\mathbf{B})^{-1}\mathbf{B}^\mathsf{T}$, to obtain sampled wave $e^{j2\pi\mathsf{ft}}e^{j2\pi\boldsymbol{f}^\mathsf{T}\boldsymbol{n}}$. Replacing $\boldsymbol{f}$ with $\boldsymbol{f}+\boldsymbol{k}$, with $\boldsymbol{k}$ any integer two-vector, changes nothing, so ranging $\boldsymbol{f}$ over any unit square accounts for all possible sampled waves.

The signal output by the element at $\mathbf{x}=\lambda\mathbf{B}\boldsymbol{n}$ takes form

$$s_{\boldsymbol{n}}(\mathsf{t}) = \iint_{\substack{\text{any unit}\\\text{square}}} \int \mathsf{S}(\boldsymbol{f},\mathsf{f})\,e^{j2\pi\mathsf{ft}}d\mathsf{f}\ e^{j2\pi\boldsymbol{f}^\mathsf{T}\boldsymbol{n}}d\boldsymbol{f} \qquad (1)$$

with $d\boldsymbol{f}$ differential area. Eigenvalue $\mathsf{S}(\boldsymbol{f},\mathsf{f})$ includes effects of the embedded element pattern and any signal processing at or referred back to the elements, notably analytic filtering (referred from DSP) to remove $\mathsf{f}<0$ components and so resolve the sign ambiguity relating $\underline{\boldsymbol{\ell}}$ to DOA. Helmholtz condition $\|\boldsymbol{\ell}\|=|\mathsf{f}|/c$ implies $\|\underline{\boldsymbol{\ell}}\|\leq|\mathsf{f}|/c$, so a "Helmholtz circle" in $\underline{\boldsymbol{\ell}}$ contains the support of "spectrum" $\mathsf{S}(\boldsymbol{f},\mathsf{f})=S(\mathbf{B}^\mathsf{T}\underline{\boldsymbol{\ell}},\mathsf{f})$.

Using 1D Fourier pair $S(\boldsymbol{f},\mathsf{t})\overset{\mathrm{CT}}{\leftrightarrow}\mathsf{S}(\boldsymbol{f},\mathsf{f})$ to rewrite (1) as

$$s_{\boldsymbol{n}}(\mathsf{t}) = \iint_{\substack{\text{any unit}\\\text{square}}} S(\boldsymbol{f},\mathsf{t})\,e^{j2\pi\boldsymbol{f}^\mathsf{T}\boldsymbol{n}}d\boldsymbol{f} \qquad (2)$$

makes $s_{\boldsymbol{n}}\overset{\mathrm{DT}}{\leftrightarrow}S(\boldsymbol{f})$ a 2D discrete-"time" Fourier pair. Dropping t-dependence notationally, the array output sought is s_0 of (2) with $S(\boldsymbol{f})$ scaled using some Fourier pair $h_{\boldsymbol{n}}\overset{\mathrm{DT}}{\leftrightarrow}H(\boldsymbol{f})$:

$$\langle\text{output}\rangle = \iint_{\substack{\text{any unit}\\\text{square}}} H(\boldsymbol{f})\,S(\boldsymbol{f})\,d\boldsymbol{f} = \big[s_{\boldsymbol{n}}*h_{\boldsymbol{n}}\big]_{\boldsymbol{n}=0}$$

$$= \Big[\sum_{\boldsymbol{m}} s_{\boldsymbol{m}}h_{\boldsymbol{n}-\boldsymbol{m}}\Big]_{\boldsymbol{n}=0} = \sum_{\boldsymbol{m}} s_{\boldsymbol{m}}h_{-\boldsymbol{m}}. \qquad (3)$$

The *array taper* is 2D FIR-filter impulse response $h_{\boldsymbol{n}}$, and $H(\boldsymbol{f})=H(\mathbf{B}^\mathsf{T}\underline{\boldsymbol{\ell}})=H(\mathbf{B}^\mathsf{T}\boldsymbol{\ell})$ is the *array factor*. Or use $h_{\boldsymbol{n}}e^{j2\pi\boldsymbol{\ell}_s^\mathsf{T}\mathbf{B}\boldsymbol{n}}\overset{\mathrm{DT}}{\leftrightarrow}H(\boldsymbol{f}-\mathbf{B}^\mathsf{T}\boldsymbol{\ell}_s)=H(\mathbf{B}^\mathsf{T}(\underline{\boldsymbol{\ell}}-\underline{\boldsymbol{\ell}}_s))$ to steer to $\underline{\boldsymbol{\ell}}_s$.

2.2 Specific array and array-factor assumptions

Square plots in figures below depict the origin-centered $\underline{\boldsymbol{\ell}}$ plane with array boresight into the page. Azimuth and elevation increase rightward and upward respectively. The first and second basis-vector columns of $\mathbf{B}$ point rightward and downward 60° respectively (as later drawn over the contour plot in Fig. 3, second row left). Basis-vector lengths space elements at $\lambda/\sqrt{3}$ to just avoid spatial aliasing for arbitrary steering (just as $\lambda/2$ would for orthogonal basis vectors).

Here complex weights $h_{\boldsymbol{n}}$ are made real—the array-factor conjugate symmetry is harmless—and are normalized

to set $H(0) = 0$. Further, $H(\mathbf{B}^\mathrm{T}\boldsymbol{\ell})$ is given the same twelve-fold symmetry with respect to rotations and reflections that the element-position grid has, simply to take computational advantage of the twelvefold symmetry that then results in h_n.

3. THE TAPERS

Array-factor plot conventions are discussed here, ahead of Figs. 3 and 4 to which they apply, as they are common to all discussions below. For each array factor, $20 \log_{10} |H(\mathbf{B}^\mathrm{T}\boldsymbol{\ell})|$ is plotted. Each 2D plot shows elevation and azimuth on the Helmholtz circle as latitude and longitude respectively using $10°$ grid lines, or as marked in zoomed views. The unit square is a period of $H(\boldsymbol{f})$, so the hexagon circumscribing the unit circle is a period of array factor $H(\mathbf{B}^\mathrm{T}\boldsymbol{\ell})$. Lines rightward and upward from origin to edge correspond to nearby plots of array factor magnitude along those slices. The taper loss

$$-10 \log_{10} \frac{|H(0)|^2}{\|h\|^2 N}$$

is the boresight SNR penalty relative to the uniform-weighting optimum given uncorrelated white noise of common spectral height at the elements, presumably from preamps. The N nonguard elements have $h_n \neq 0$. Notation $\|h\|^2 = \sum_n |h_n|^2$, the energy in function h_n.

3.1 A Hexagonal Array

Here three taper-design approaches are compared for a 9,919 element hexagonal array that extends to "radius" 57 this

array of "radius" two ⬢.

Such a hexagonal array results by construction from one approach, the three-way product taper. The McClellan transformation is less restricted but performs best for a hexagonal array. The optimal approach has no array-shape restriction.

Results for these three designs will be presented in Fig. 3.

3.1.1 The McClellan transformation

McClellan transformation [2] of a 1D prototype into a 2D filter, well known in image processing, is based on [3] viewing the impulse response of a real zero-phase filter in 1D as a linear combination of basis functions. The first two are a unit impulse at the origin and a discrete-time "spreading function" x_n comprising unit impulses at $n = \pm 1$, and the others

$$
\begin{aligned}
\phi_n^0 &= \delta_n \\
\phi_n^1 &= x_n \\
\phi_n^2 & \\
\phi_n^3 & \\
\phi_n^4 & \\
&\vdots
\end{aligned}
$$
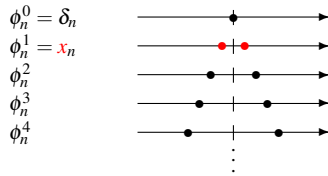
are created using[1] the recursion $\phi_n^k = \phi_n^{k-1} * x_n - \phi_n^{k-2}$ or its equivalent, $\Phi^k(\mathsf{f}) = \Phi^{k-1}(\mathsf{f}) X(\mathsf{f}) - \Phi^{k-2}(\mathsf{f})$. A real 1D zero-phase prototype filter then has responses of the form

$$h_n = \sum_{k=0}^{\infty} h_k \phi_n^k \overset{\mathrm{DT}}{\leftrightarrow} \sum_{k=0}^{\infty} h_k \Phi^k(\mathsf{f}) = H(\mathsf{f}).$$

[1] The spreading function and recursions are usually scaled differently so that the frequency-domain recursion yields Chebyshev polynomials, but that normalization is actually immaterial unless the recursion is used in filter implementation—here they are not—and this development is cleaner.

By construction, these $\Phi^k(\mathsf{f})$ and therefore $H(\mathsf{f})$ depend on f only through $X(\mathsf{f})$, so $H(\mathsf{f})$ can be written in form $G(X(\mathsf{f}))$.

The McClellan transformation replaces 1D Fourier pair $x_n \overset{\mathrm{DT}}{\leftrightarrow} X(\mathsf{f})$ above with some 2D Fourier pair $x_n \overset{\mathrm{DT}}{\leftrightarrow} X(\boldsymbol{f})$ to obtain a 2D filter from the 1D prototype. The same recursion and weights now yield 2D pair $h_n \overset{\mathrm{DT}}{\leftrightarrow} H(\boldsymbol{f}) = G(X(\boldsymbol{f}))$ and therefore both the array taper and array factor $G(X(\mathbf{B}^\mathrm{T}\boldsymbol{\ell}))$. Function G is the same, so f and $\boldsymbol{\ell}$ with $X(\mathbf{B}^\mathrm{T}\boldsymbol{\ell}) = X(\mathsf{f})$ yield $H(\mathbf{B}^\mathrm{T}\boldsymbol{\ell}) = G(X(\mathbf{B}^\mathrm{T}\boldsymbol{\ell})) = G(X(\mathsf{f})) = H(\mathsf{f})$, resulting in the key to the approach: array factor $H(\mathbf{B}^\mathrm{T}\boldsymbol{\ell})$ at $\boldsymbol{\ell}$ has the same value as filter frequency response $H(\mathsf{f})$ at $\mathsf{f} = X^{-1}(X(\mathbf{B}^\mathrm{T}\boldsymbol{\ell}))$.

Here $X(\mathbf{B}^\mathrm{T}\boldsymbol{\ell})$ is in effect the array factor of a tiny array. This choice maximizes the number of degrees of design freedom (basis functions used) given required array symmetry:

weight $-2/3$ on center "element"
weight $4/9$ on outer "elements"

The contour plot in the second row of Fig. 3 shows these normalized positions $\mathbf{B}n$ on the same scale as the basis vectors, with index vector n shown to the left of each position.

The map from the 1D prototype response $H(\mathsf{f})$, top plot dark line, to array factor $H(\mathbf{B}^\mathrm{T}\boldsymbol{\ell})$, left end of bottom two rows on two scales, is represented by contours of $\mathsf{f} = X^{-1}(X(\mathbf{B}^\mathrm{T}\boldsymbol{\ell}))$ as a function of $\boldsymbol{\ell}$. To design prototype $H(\mathsf{f})$, the Opt toolbox [4] is first used to formulate a small SOCP much like the small-spreading-function example of [3, Section 3.3.4], the best performing of that preliminary exploration. This SOCP minimizes the taper loss of transformed 2D array factor $H(\mathbf{B}^\mathrm{T}\boldsymbol{\ell})$ subject to constraints fixing $H(0) = 1$ and, at many closely spaced frequencies f, upper bounding $20 \log_{10} |H(\mathsf{f})|$ by the top plot's piecewise-straight line extending from -30 dB at $\mathsf{f} = 0.015$ to -50 dB at $\mathsf{f} = 0.237$, where it levels off. The contours map this leveling-off frequency roughly to a a $30°$ radius circle in $\boldsymbol{\ell}$. The SOCP is solved numerically with SeDuMi [5, 6]. On an ordinary notebook computer the Opt setup and SeDuMi solution of the SOCP together take about four seconds, which is less than required to compute basis functions $\phi_n^0, \ldots, \phi_n^{57}$.

3.1.2 Three-way product taper

Specify three array-plane vectors $\widehat{u}_i \triangleq \frac{1}{2}\mathbf{B}^{+\mathrm{T}}\boldsymbol{k}_i$ and verify that they are unit vectors equally spaced in angle:

$$\boldsymbol{k}_1 = \begin{bmatrix} 1 \\ 1 \end{bmatrix}, \quad \boldsymbol{k}_2 = \begin{bmatrix} -1 \\ 0 \end{bmatrix}, \quad \boldsymbol{k}_3 = \begin{bmatrix} 0 \\ -1 \end{bmatrix},$$

$$\langle \widehat{u}_i, \widehat{u}_j \rangle = \tfrac{1}{4}\boldsymbol{k}_i^\mathrm{T}\mathbf{B}^+\mathbf{B}^{+\mathrm{T}}\boldsymbol{k}_j = \tfrac{1}{4}\boldsymbol{k}_i^\mathrm{T}(\mathbf{B}^\mathrm{T}\mathbf{B})^{-1}\boldsymbol{k}_j$$

$$= \boldsymbol{k}_i^\mathrm{T} \tfrac{1}{2}\begin{bmatrix} 2 & -1 \\ -1 & 2 \end{bmatrix}\boldsymbol{k}_j = \begin{cases} 1 & \text{if } i = j \\ -\tfrac{1}{2} & \text{if } i \neq j. \end{cases}$$

Heavy arrows $\widehat{u}_1$, $\widehat{u}_2$, and $\widehat{u}_3$ in the λ-normalized Fig. 1 array plane are normal to alternate sides of the hexagonal array. Element rows are effectively numbered in the $\widehat{u}_i$ direction by twice the projection onto $\widehat{u}_i$ of λ-normalized nominal element location $\mathbf{x}/\lambda = \mathbf{B}n$ or $2\widehat{u}_i^\mathrm{T}\mathbf{x}/\lambda = \boldsymbol{k}_i^\mathrm{T}\mathbf{B}^+\mathbf{B}n = \boldsymbol{k}_i^\mathrm{T}n$. Define matrix $\mathbf{K}$ to combine these row indices into a vector:

$$\mathbf{K}n = \begin{bmatrix} \boldsymbol{k}_1^\mathrm{T} \\ \boldsymbol{k}_2^\mathrm{T} \\ \boldsymbol{k}_3^\mathrm{T} \end{bmatrix} n = \begin{bmatrix} 1 & 1 \\ -1 & 0 \\ 0 & -1 \end{bmatrix} n.$$

Now define a Fourier pair in 3D using notation

$$s_\mathbf{m} \overset{\mathrm{DT}}{\leftrightarrow} S(\mathbf{f}), \qquad \mathbf{m} \triangleq \begin{bmatrix} m_1 \\ m_2 \\ m_3 \end{bmatrix}, \qquad \mathbf{f} \triangleq \begin{bmatrix} f_1 \\ f_2 \\ f_3 \end{bmatrix}.$$
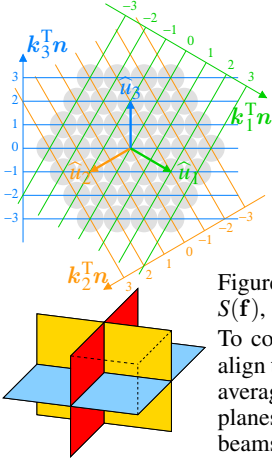
Figure 1: Three-way product taper $h_n = q_{k_1^T n} \, q_{k_2^T n} \, q_{k_3^T n}$ uses counts of element rows in equally spaced directions $\hat{u}_1$, $\hat{u}_2$, and $\hat{u}_3$ defined by integer two-vector constants k_1, k_2, and k_3 to index into some 1D taper q_m.
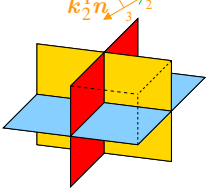

Figure 2: A 3D period of separable function $S(\mathbf{f})$, with planes for main beams of $Q(f_i)$. To construct array factor $H(\mathbf{B}^T \underline{\ell})$, rotate to align the dotted corner above its opposite and average vertically. An intersection of two planes has two of three $Q(f_i)$ factors in main beams and creates a "ray" in the average.

We can use a 1D taper q_n to write $s_{\mathbf{m}} \triangleq q_{m_1} q_{m_2} q_{m_3}$ if $s_{\mathbf{m}}$ is separable and identical in each dimension. Then $S(\mathbf{f})$ is also separable: $S(\mathbf{f}) = Q(f_1) Q(f_2) Q(f_3)$ using $q_m \overset{\text{DT}}{\leftrightarrow} Q(f)$ in 1D. We construct product taper $h_n = s_{\mathbf{K}n} = q_{k_1^T n} q_{k_2^T n} q_{k_3^T n}$.

The taper fixes array factor $H(\mathbf{B}^T \underline{\ell})$ and makes computation simple. To predict its general look. write Fourier integral

$$s_{\mathbf{m}} = \int_{\substack{\text{any unit} \\ \text{cube}}} S(\mathbf{f}) e^{j2\pi \mathbf{f}^T \mathbf{m}} d\mathbf{f} = \underset{\mathbf{f}}{\text{avg}} \left\{ S(\mathbf{f}) e^{j2\pi \mathbf{f}^T \mathbf{m}} \right\}$$

using an "average over $\mathbf{f}$" notation to hide the tedious details of upcoming change of variable $\mathbf{f} = \mathbf{K}^{+T} f + \mathbf{f}_\perp$, where f is a 2D coordinate vector and 3D vector $\mathbf{f}_\perp$ is normal to the columns of both $\mathbf{K}^{+T}$ and $\mathbf{K}$. Changing variables yields

$$s_{\mathbf{m}} = \underset{f}{\text{avg}} \left\{ \underset{\mathbf{f}_\perp}{\text{avg}} \left\{ S(\mathbf{K}^{+T} f + \mathbf{f}_\perp) e^{j2\pi (\mathbf{K}^{+T} f + \mathbf{f}_\perp)^T \mathbf{m}} \right\} \right\}$$

so that, using $\mathbf{K}^+ \mathbf{K} = \mathbf{I}$ and $\mathbf{f}_\perp^T \mathbf{K} = 0$, our taper becomes

$$h_n = s_{\mathbf{K}n} = \underset{f}{\text{avg}} \left\{ H(f) e^{j2\pi f^T n} \right\} = \int_{\substack{\text{any unit} \\ \text{square}}} H(f) e^{j2\pi f^T n} df,$$

$$H(f) = \underset{\mathbf{f}_\perp}{\text{avg}} \left\{ S(\mathbf{K}^{+T} f + \mathbf{f}_\perp) \right\} \qquad (4)$$

and thus almost establishes that $h_n \overset{\text{DT}}{\leftrightarrow} H(f)$ is the usual Fourier pair in 2D and therefore that (4) yields array taper

$$H(\mathbf{B}^T \underline{\ell}) = \underset{\mathbf{f}_\perp}{\text{avg}} \left\{ S(\mathbf{K}^{+T} \mathbf{B}^T \underline{\ell} + \mathbf{f}_\perp) \right\}. \qquad (5)$$

"Almost" is because the required periodicity of $H(f)$ is so far unproven, but the Fig. 1 geometry in fact implies it. Zero results when boresight vector $[1\ 1\ 1]^T$ is left multiplied by

$$\mathbf{K}^{+T} \mathbf{B}^T = \frac{1}{3\sqrt{6}} \begin{bmatrix} -2 & -1 & 1 \\ 1 & -2 & 1 \\ 1 & 1 & -2 \end{bmatrix}$$

and this matrix's other two eigenvalues are nonzero and identical: map $\underline{\ell} \mapsto \mathbf{K}^{+T} \mathbf{B}^T \underline{\ell}$ is scaling and array-plane rotation.

This formalism illumines array-factor behavior. In (5) separable, periodic 3D frequency response $S(\mathbf{f})$ is first oriented to stand each unit-cube period on a corner and orient boresight-direction vector $[1\ 1\ 1]^T$ vertically. Averaging out that vertical dimension then yields a 2D response on the horizontal plane. Finally the horizontal plane is rotated and scaled to correct array-factor orientation and periodicity.

The example array factor $H(\mathbf{B}^T \underline{\ell})$ in Fig. 3 (center column) was created from a 115-sample Taylor taper q_m with $\bar{n} = 4$ and a -23 dB sidelobe limit. The red curve (top, upper curve in sidelobes) displays $|Q(f)|$ in dB for $0 \le f \le \frac{1}{2}$.

Six "rays" in $H(\mathbf{B}^T \underline{\ell})$ are inevitable, as per Fig. 2. For example, along the $\mathbf{f}$ line where $\mathbf{f} = [0\ 0\ f_3]^T$, only $Q(f_3)$ contributes attenuation to $S(\mathbf{f})$, so that line dominates the average and forms a ray. The Taylor parameters chosen roughly match sidelobe levels in the rays to those of the example McClellan-transformation design. On the lower right of Fig. 3 array-factor magnitude is plotted in dB versus each of azimuth and elevation with the other fixed at zero.

3.1.3 SOCP optimization

An auxiliary variable δ and the 870 real variables required, given the taper's constructed-in symmetry, to characterize taper h_n are jointly optimized to minimize δ subject to

second-order cone constraint $\quad \|h\| \le \delta,$

linear constraint $\quad H(0) \ge 1,$ and

linear constraint pairs $\quad -b_i \le H(\mathbf{B}^T \underline{\ell}_i) \le b_i, \quad (6)$

the latter for $i = 1, \ldots, 16846$ with these many $\underline{\ell}_i$ comprising a carefully designed fine mesh across $\frac{1}{12}$ of the sidelobe region. The rest of the sidelobe region is constrained implicitly, as the symmetry constructed into h_n implies twelvefold symmetry in $H(\mathbf{B}^T \underline{\ell})$. Decibel bound $20 \log_{10} b_i$ depends on $\|\underline{\ell}_i\|$ only and ramps from -30 dB at $\|\underline{\ell}_i\| = \sin 1.75°$ to -50 dB at $\|\underline{\ell}_i\| = \sin 30°$, where it remains for larger $\|\underline{\ell}_i\|$.

This SOCP is solved using the Opt [4] matlab-toolbox interface to the SeDuMi [5, 6] solver and yields the array factor of Fig. 3 (right column). Zero-azimuth and zero-elevation slices are plotted in the lower right. Sidelobe suppression is most difficult in directions along which the array is narrower, and along rays in those directions bounds (6) become active.

Solution on an ordinary linux-based notebook computer requires about 15 minutes. Large SOCP array optimizations tend to be memory bound, and here the 4 Gbytes of main memory is indeed fairly fully used (without paging to disk).

3.2 A Circular Array

Figure 4 compares two tapers for the 9,913-element circular array of elements at those positions $\mathbf{x} = \lambda \mathbf{B} n$ for which $\|\mathbf{x}\|^2 \le \frac{2725}{3} \lambda^2$. The circular geometry eliminates rays and better uses the degrees of design freedom but is incompatible with the McClellan transformation and the three-way product. The simple approach is to sample a continuous aperture.

3.2.1 Sampling a continuous aperture

The example array factor in Fig. 4 (center column) samples Taylor's classic circular aperture [1], a continuous 2D taper, at each element position $\mathbf{x} = \lambda \mathbf{B} n$ using $\|\mathbf{x}\|$ and the maximum it attains respectively as Taylor's radial position ρ and aperture radius a. His sidelobe-level parameter η is set for $20 \log_{10} \eta = 30$ dB, the center of the range tabulated in detail by Hansen [7], and Schrank's [8] so-called optimum $\bar{n}$ for this η is used: $\bar{n} = 4$. Hansen's tables coarsely sampling the distribution across the aperture serve as a check on the code.

3.2.2 SOCP optimization

Optimization of the Fig. 4 example (right column) is largely as in Section 3.1.3 but with the constraint ramp modified to reach -50 dB at $\|\underline{\ell}_i\| = \sin 12°$ to ease comparison with the sampled-aperture design. Solving takes 25 minutes due to tight constraints with few unused degrees of freedom. (Arrays $\frac{1}{4}$ this size often optimize in under a minute.)
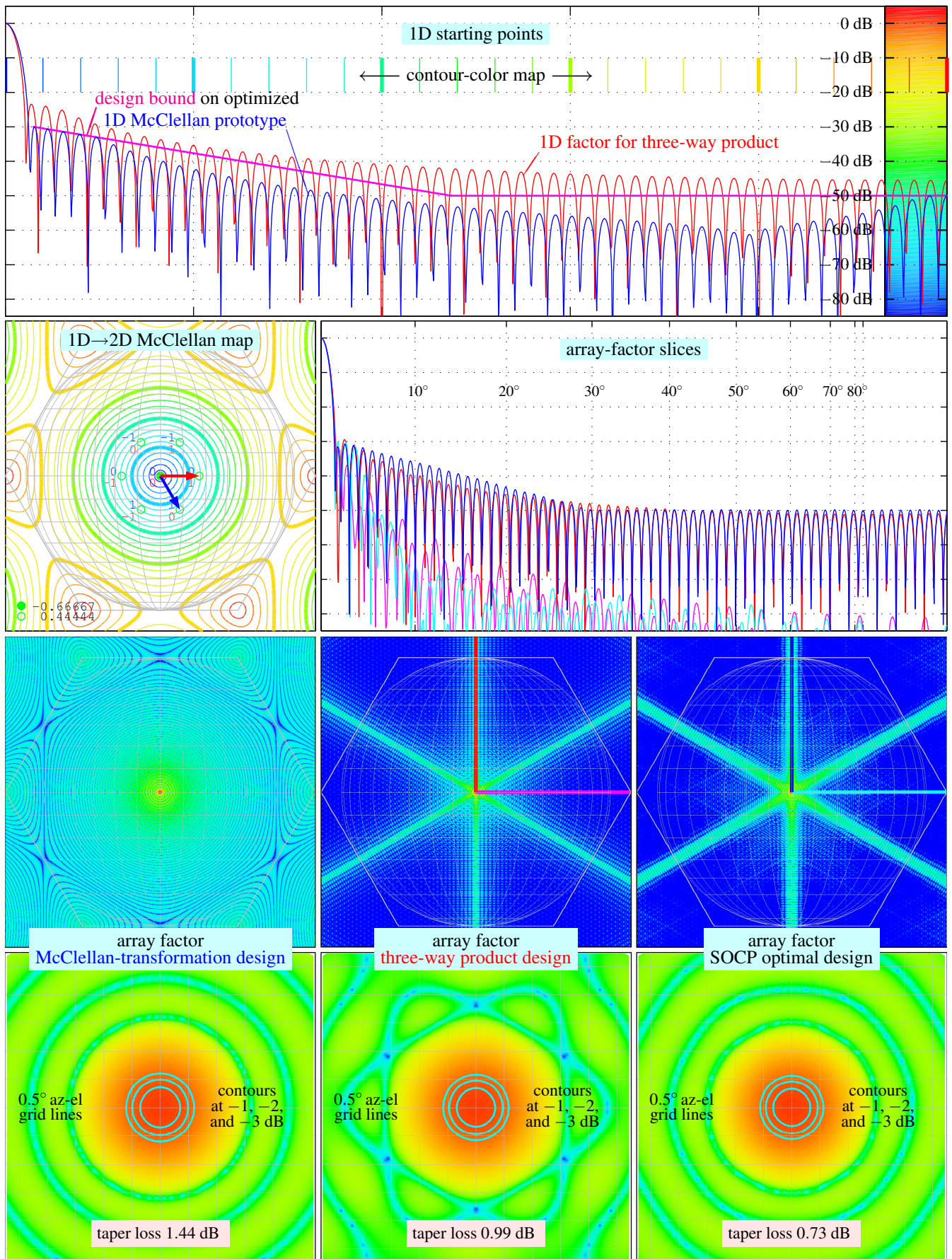
Figure 3: Array factors, 9919-element hexagonal array: McClellan transform (left), three-way product (center), SOCP optimization (right).
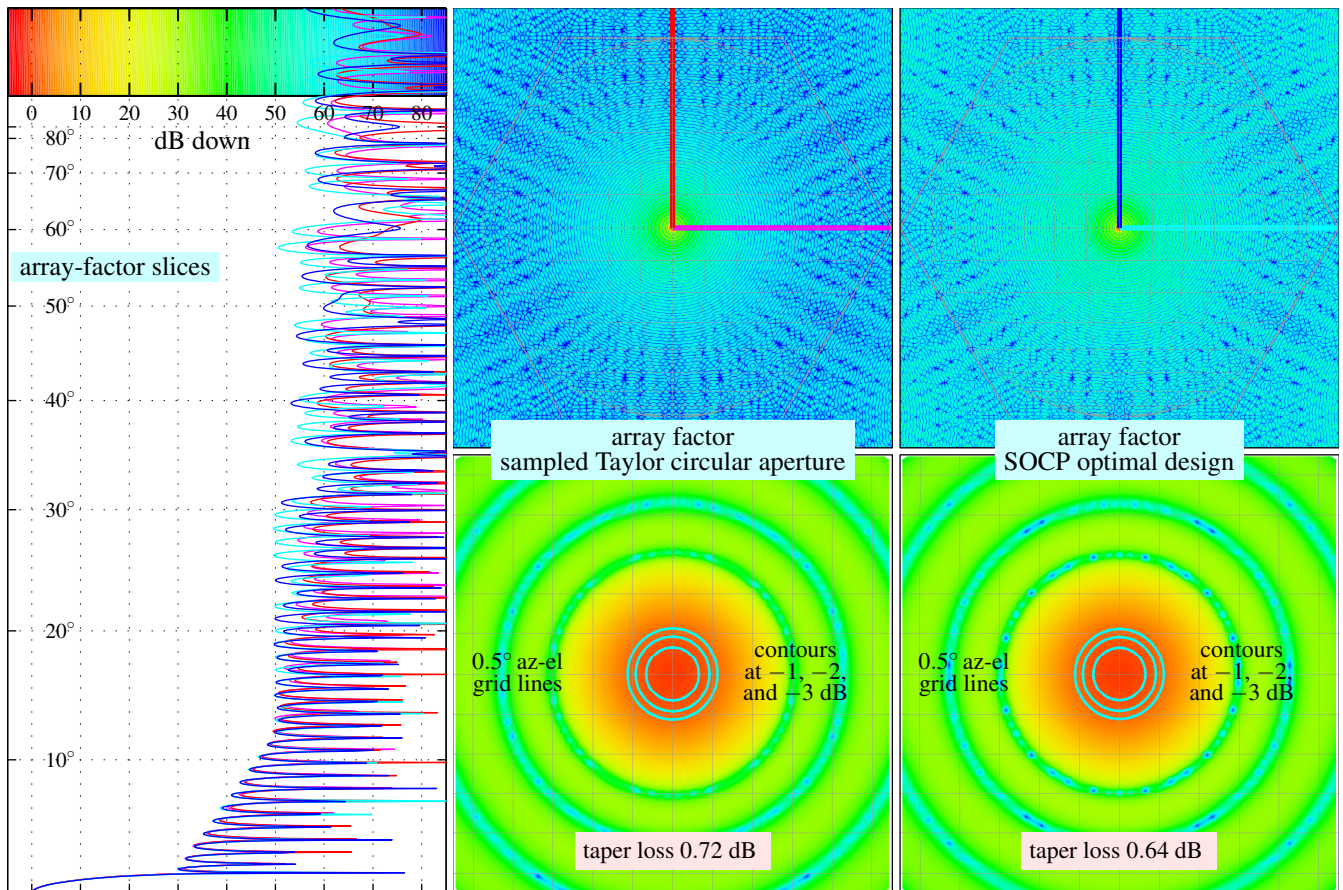
Figure 4: Array factors, 9,913-element circular array. Tapers are SOCP optimized (right) and sampled from Taylor's circular aperture (center).

4. OBSERVATIONS AND CONCLUSIONS

The Fig. 3 hexagonal-array designs suggest the McClellan transformation is unsuitable when its real-time computability [3] is not required, because its symmetry requires high sidelobes everywhere if there are high sidelobes anywhere. High ray sidelobes simply take over. The example here also has ≥ 0.45 dB more taper loss than the competing designs.

At first glance the three-way product yields reasonable results when rays can be tolerated, with only 0.26 dB more taper loss than an optimal design constrained to permit similar rays. Of course there's nothing reasonable about permitting rays. The Fig. 4 circular-array designs trade away some of the hexagonal array's needlessly excessive off-ray sidelobe rejection in order to simply remove those rays. In those designs the chosen $\bar{n}$ gives the circular-Taylor array factor aggressively attenuated inner sidelobes, and the competing optimal design was constrained to more or less match, resulting in an optimal taper-loss advantage of only 0.08 dB.

Modern optimization is so simple that it should always be tried, but its benefits are less about better performance given specs that are simple than about tradeoff flexibility when they are not. When a circular-Taylor design is in every way just adequate, that approach is reasonable. But when that yields an array factor overdesigned in some way or in some region, optimizing instead can trade away that overdesign, through crafted constraints, for better performance elsewhere. The optimal approach's flexibility particularly suits the challenging requirements of systems with main-beam or sidelobe shaping or that involve overlapping subarrays.

REFERENCES

[1] T. Taylor, "Design of circular apertures for narrow beamwidth and low sidelobes," *IRE Trans. Antennas and Propagation*, vol. 8, no. 1, pp. 17–22, Jan. 1960.

[2] J. McClellan and D. Chan, "A 2-D FIR filter structure derived from the Chebyshev recursion," *IEEE Trans. Circuits and Systems*, vol. 24, no. 7, pp. 372–378, July 1977.

[3] J. O. Coleman, "Amplitude tapers for planar arrays using the McClellan transformation: concepts and preliminary design experiments," Naval Research Laboratory, NRL Memo Report 9231, in press, release expected in late 2010.

[4] J. O. Coleman, D. P. Scholnik, and J. J. Brandriss, "A specification language for the optimal design of exotic FIR filters with second-order cone programs," in *IEEE Asilomar Conf. on Signals, Systems, and Computers*, Nov. 2002.

[5] J. F. Sturm, "Using SeDuMi 1.02, a Matlab toolbox for optimization over symmetric cones," *Optimization Methods and Software*, vol. 11–12, pp. 625–653, 1999, vers. 1.02/1.03, updated for vers. 1.05 online: http://www.optimization-online.org/DB_HTML/2001/10/395.html.

[6] I. Pólik and T. Terlaky, "SeDuMi 1.21," Cor@l Lab: Computational Optimization Research at Lehigh, taking over from SeDuMi's author, the late Jos Sturm. Project website: http://sedumi.ie.lehigh.edu/.

[7] R. Hansen, "Tables of Taylor distributions for circular aperture antennas," *IRE Trans. Antennas and Propagation*, vol. 8, no. 1, pp. 23–26, Jan. 1960.

[8] H. Schrank, "Antenna designer's notebook," *IEEE Antennas and Propagation Society Newsletter*, vol. 28, no. 4, pp. 30–31, Aug. 1986.